2010

Magnetic nanoparticles for applications in oscillating magnetic field

Chorthip Peeraphatdit
Iowa State University

Magnetic nanoparticles for applications in oscillating magnetic field

by

Chorthip Peeraphatdit

A thesis submitted to the graduate faculty

in partial fulfillment of the requirements for the degree of

MASTER OF SCIENCE

Major: Chemistry

Program of Study Committee:
Victor Shang-Yi Lin, Major Professor
Marek Pruski
Malika Jeffries-EL

Iowa State University

Ames, Iowa

2010

TABLE OF CONTENTS

ACKNOWLEDGEMENTS

I would like to take this opportunity to express my deepest gratitude for the support that I have received during these past years.

To my major advisor, Professor Victor Shang-Yi Lin, for his guidance, creativity and his unrelenting enthusiasm for science. Without his endless support and encouragements, my mental block would have been impossible to overcome.

To all my past and present POS committee members, Professor Marek Pruski, Professor Malika Jeffries-EL, Professor Keith Woo, Professor Nicola Pohl and Professor Zhiqun Lin for their guidance and for giving me a chance to learn and grow.

To Robert Vincent for giving so much of his time and energy in building the device that is crucial in this work, and also for his kind support.

To all the past and present members of the Lin group who helped through lab and life.

To all the funding agencies that supported this work, especially the U.S. Department of Energy.

ABSTRACT

Enzymatic and thermochemical catalysis are both important industrial processes. However, the thermal requirements for each process often render them mutually exclusive: thermochemical catalysis requires high temperature that denatures enzymes. One of the long-term goals of this project is to design a thermocatalytic system that could be used with enzymatic systems *in situ* to catalyze reaction sequences in one pot; this system would be useful for numerous applications e.g. conversion of biomass to biofuel and other commodity products. The desired thermocatalytic system would need to supply enough thermal energy to catalyze thermochemical reactions, while keeping the enzymes from high temperature denaturation. Magnetic nanoparticles are known to generate heat in an oscillating magnetic field through mechanisms including hysteresis and relaxational losses. We envisioned using these magnetic nanoparticles as the local heat source embedded in sub-micron size mesoporous support to spatially separate the particles from the enzymes. In this study, we set out to find the magnetic materials and instrumental conditions that are sufficient for this purpose.

Magnetite was chosen as the first model magnetic material in this study because of its high magnetization values, synthetic control over particle size, shape, functionalization and proven biocompatibility. Our experimental designs were guided by a series of theoretical calculations, which provided clues to the effects of particle size, size distribution, magnetic field, frequency and reaction medium. Materials of theoretically optimal size were synthesized, functionalized, and their effects in the oscillating magnetic field were subsequently investigated. Under our conditions, the materials that clustered e.g. silica-coated and PNIPAM-coated iron oxides exhibited the highest heat generation, while iron

oxides embedded in MSNs and mesoporous iron oxides exhibited the least bulk heating. It is worth noting that the specific loss power of PNIPAM-coated Fe_3O_4 was peculiarly high, and the heat loss mechanism of this material remains to be elucidated.

Since thermocatalysis is a long-term goal of this project, we also investigated the effects of the oscillating magnetic field system for the synthesis of *7*-hydroxycoumarin-3-carboxylic acid. Application of an oscillating magnetic field in the presence of magnetic particles with high thermal response was found to effectively increase the reaction rate of the uncatalyzed synthesis of the coumarin derivative compared to the room temperature control.

CHAPTER 1. GENERAL INTRODUCTION AND THEORETICAL OPTIMIZATION OF MAGNETIC NANOPARTICLES FOR MAGNETIC HYPERTHERMIA

Thesis organization

This thesis is divided into three chapters. Chapter 1 provides the general introduction to magnetic hyperthermia and explains the theoretical predictions of the effect. Chapter 2 describes the synthesis and characterization of various magnetic materials for evaluation under the oscillating magnetic field. Chapter 3 reports the *in vitro* hyperthermia effect from the magnetic materials under oscillating magnetic field and the effect of hyperthermia heating on the synthesis of a coumarin derivative.

General introduction

Magnetic hyperthermia

Hyperthermia therapy is a type of cancer treatment in which the body tissue is exposed to high temperature of 42 ^{o}C or higher, which is found to be more harmful to cancer cells than to normal healthy cells. Mild hyperthermia is performed at 41-46 ^{o}C to stimulate the immune response for non-specific immunotherapy of cancers, while thermoablation is performed at 46-56 ^{o}C to kill cancer cells by direct cell necrosis, coagulation or carbonization.[1] The challenge of this cancer therapy lies in controlling the heating effect to only the local tumor site so as to not harm the nearby healthy cells. To this end, magnetic hyperthermia has emerged as one of the most promising approaches for heat localization.

Magnetic hyperthermia treatment is based upon the idea that magnetic nanoparticles heat up under oscillating magnetic field. For this therapy, biocompatible magnetic nanoparticles are introduced into the tumor site either by direct injection or by targeted delivery. Oscillating magnetic field, or magnetic field generated by sending alternating current through a coil, is applied and magnetic nanoparticles interact with this field to generate heat through various mechanisms (see below).

The concept of magnetic materials in hyperthermia was first proven in 1957 when Gilchrist and co-workers heated various tissue samples with 20–100 nm size particles of γ-Fe_2O_3 exposed to a 1.2 MHz magnetic field.[2] Since then, much progress have been made in the field using various types and sizes of magnetic materials, magnetic field strengths and frequencies, methods of preparation, coatings, and nanoparticle delivery.[3,4] In 2007, Jordan and coworkers have reported the first clinical study of magnetic hyperthermia, showing that aminosilane-coated superparamagnetic iron oxide nanoparticles could be safely applied for the treatment of brain tumors, achieving hyperthermic temperatures while being well tolerated by patients.[5] However, evaluation of patient survival and local tumor control remained to be evaluated in phase II of the study.

From magnetic hyperthermia to integrated enzymatic - thermocatalytic system

Enzymes are highly specialized proteins that are capable and responsible for catalyzing biochemical reactions in cells. These biological catalysts are important due to their inherent stability, reactivity in aqueous environment, and their specificity to substrates. They also often operate at milder conditions than other classes of chemical catalysts. Various enzymatic processes are currently being used and investigated for conversion of

biomass into biofuels.[6,7] Despite these benefits, biocatalysts often yield a mixture of products that contains useful "chemical precursors" to fuels and value-added compounds. Tedious separation and refinery processes are still necessary before the final thermochemical catalytic conversion of these "biologically-derived" molecules to the desired products. The ability to marry these two processes would certainly be advantageous.[8,9]

One of the long-term goals in our research group is to develop a 'reactor' that combines biological and thermochemical catalysis into a one-pot reaction sequence (Figure 1-1). In this system, the reactant of interest is converted by an enzyme or microbes into a stable intermediate, which is then thermochemically converted to the final product using multifunctional mesoporous silica nanoparticle (MSN) catalyst. The energy required for the thermochemical step is supplied by magnetic nanoparticles embedded within the matrix of the high surface material that become activated by an oscillating magnetic field, inducing the magnetic hyperthermia effect.

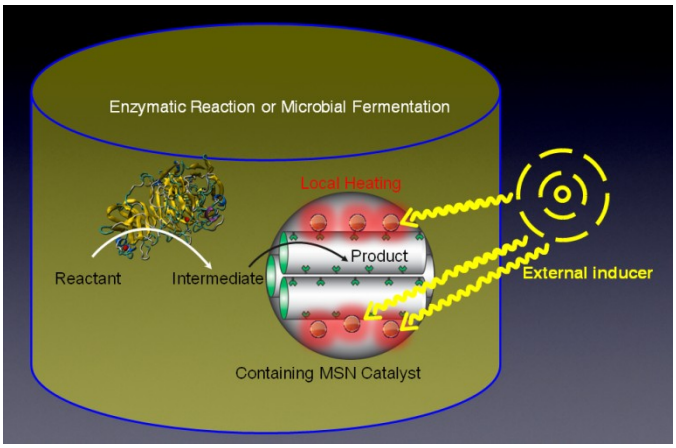

Figure 1-1. Schematic representation of the induction of thermochemical catalysis in biological systems. Oscillating magnetic field triggers local heating of multifunctional nanoparticles-containing mesoporous catalyst.

To achieve this goal, the following key requirements must be met:

1. A large amount of heat must be locally generated for the thermochemical system while protecting the enzymes from denaturation.
    - The support will prevent direct contact between the nanoparticle heat source and the enzyme.
2. The catalytic site should be in close proximity with the source of local heating.
    - The catalytic groups and the thermoactive nanoparticles, such as those depicted in Figure 1-1, can be incorporated in different domains of a sub-micron sized support with a high surface area. If the local heat sources (nanoparticles) are embedded within the matrix of the support and the catalytic groups are located in its surface, the thickness of the walls of the support provides the spatial separation between these two components.
3. Catalyst and support should be biocompatible in the case of microbial fermentation. In this study, both the iron oxide nanoparticles and the MSN support have been proven biocompatible.

In this work, we first set out to fulfill the first requirement by identifying suitable magnetic materials that can generate sufficient heat under oscillating magnetic field and the instrumental conditions that promote this effect. In addition, the effects of functionalization and immobilization of the magnetic nanoparticles will also be investigated.

Types of magnetic materials

Magnetic behavior of bulk materials generally falls into 5 categories: diamagnetism, paramagnetism, ferromagnetism, antiferromagnetism, and ferrimagnetism. Since the

magnetic susceptibilities of diamagnetic, paramagnetic and antiferromagnetic materials are weak, only the other 2 categories are useful for magnetic applications.[10]

Ferromagnetism is present in materials like iron, nickel and cobalt, whose atomic moments have very strong interactions and exhibit parallel alignment (Figure 1-2a), resulting in a large net magnetization even in the absence of a magnetic field (spontaneous magnetization). Ferromagnetic materials exhibit long-range magnetic order below the Curie temperature, where the magnetic order is overcome by thermal energy and they become paramagnetic.

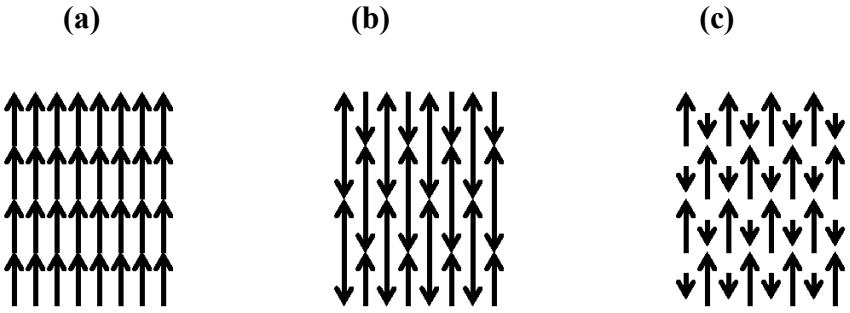

Figure 1-2. Magnetic ordering in (a) ferromagnetic, (b) antiferromagnetic, and (c) ferrimagnetic materials.

Ferrimagnetism is similar to antiferromagnetism in that the magnetic moments align in the opposite directions; however, in this type of material, the opposing moments are unequal resulting a net magnetic moment and thus spontaneous magnetization (Figure 1-2c). Some examples of ferrimagnetic materials are magnetite and most ferrites e.g. cobalt ferrite, nickel ferrite, and manganese ferrite. Ferrimagnetic materials also become paramagnetic at or above the Curie temperature.

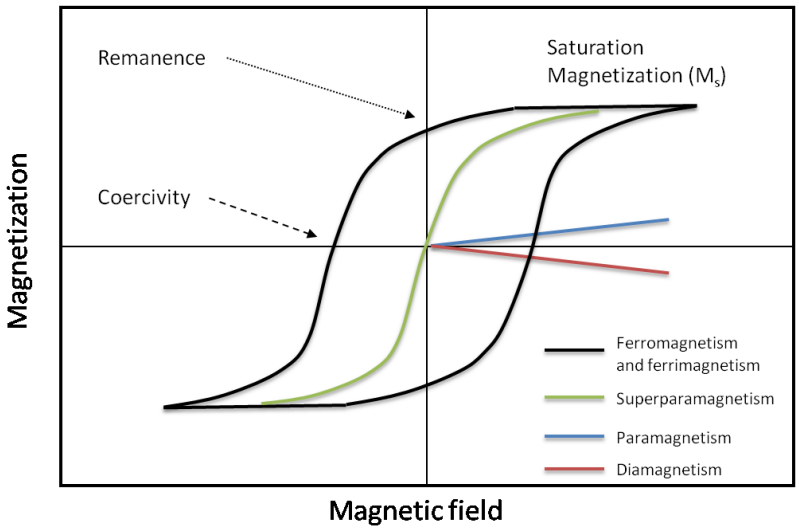

Figure 1-3. Magnetization versus applied magnetic field representative for different classes of magnetism.

Both ferromagnetic and ferrimagnetic materials exhibit a behavior called hysteresis, meaning that they can retain a memory of an applied field after it has been removed. The hysteresis loop or plot of magnetization with magnetic field for these materials is shown in Figure 1-3. The hysteresis loop shows that the magnetization of both materials can increase with increasing applied field up to a point, called the saturation magnetization. However, when the field is removed, the magnetization is retained; even as the field is reduced to zero, remanence magnetization is retained due to the hysteresis. To reduce the magnetization back to zero, some amount of magnetic field of opposite direction has to be applied; this field is termed coercivity.

Given the above description, one might expect ferromagnetic and ferrimagnetic materials to always exhibit large total magnetic moment. However, this is not the case because these materials naturally divide their structure into smaller regions, called domains. In each domain, magnetic moments are aligned in a direction that is different from

neighboring domains, which lowers the magnetization of the overall structure. Domain structures are favorable because they help lower the magnetostatic energy. However, creating and maintaining domain walls (the transition regions between the domains) also requires energy. Thus, the number of domains required depends on the balance between these two competing factors.

As we shrink the grain size, a critical size is reached where domain walls can no longer be accommodated and the whole grain behaves as a single domain. Single domain particles have large hysteresis loops with high coercivity and remanence. However, as we continue to shrink the grain size, another critical size is reached where the coercivity and remanence goes to zero and the particle becomes superparamagnetic. Superparamagnetic materials do not exhibit any hysteresis (Figure 1-3).

Superparamagnetism generally occurs in the nanometer size range; the critical size depends on the type of the material and temperature. In the absence of the magnetic field, thermal energy causes magnetic moments of the superparamagnetic particles to fluctuate, resulting in zero net magnetic moment. In the magnetic field, single domain particles align, similarly to individual atoms in a paramagnetic material, resulting in a giant global magnetic moment.

Mechamisms of heat generation

In order to find the materials suitable for the thermocatalytic system as mentioned above, the knowledge and understanding of the heating mechanism is essential. Magnetic nanoparticles can generate heat under oscillating magnetic field via various mechanisms

including hysteresis loss, [11] Néel relaxation and Brown relaxation.[12] The type and size of the materials determine which mechanism predominates.

Multidomain ferromagnetic and ferrimagnetic materials typically exhibit hysteresis loss, due to irreversible domain wall displacements during the application of oscillating magnetic field. However, it is difficult to harness the full potential of the hysteresis loss because of the technical restriction on field amplitude and the fact that they vanish in single domain, smaller particles.[1] The single domain superparamagnetic nanoparticles, on which our current work is focused (see below), possess global magnetic moments that align with the applied magnetic field. When the field is removed, the magnetic moments relax either by internal fluctuation (Néel relaxation) or by rotation of the whole particle (Brown relaxation). The contribution of each relaxation loss depends on the anisotropy constant and size of the material, and viscosity of the medium. An application of oscillating magnetic field provides energy for sustaining the relaxation processes, which result in dissipation of thermal energy.

Many factors can influence the amount of heat, termed specific loss power (SLP), released through magnetic relaxation. These factors include types of material and its magnetization, size and shape of material, frequency and strength of the applied magnetic field, and the medium in which the particles are suspended.[11,13] Using the theoretical calculations as outlined below, we can determine the size of materials and the instrumental conditions that will maximize heat loss under the oscillating magnetic field.

Theoretical optimization of magnetic nanoparticles for magnetic hyperthermia

SLP equations

Assuming small single domain superparamagnetic nanoparticles, the SLP in an oscillating magnetic field can be predicted using the following set of equations:[14,15]

$$\mathrm{SLP} = \frac{\mathrm{P}}{\rho\phi} = \frac{\mu_o \chi_o H_o^2}{2\rho\phi}\omega\frac{\omega\tau}{1+(\omega\tau)^2} \quad (1)$$

where P is The mean volumetric power dissipation, μ_0 is the permeability of free space, χ_0 is the magnetic susceptibility, H_0 the magnetic field strength, ω the angular frequency ($\omega = 2\pi f$), τ the effective relaxation time, ρ the density of the material and ϕ the volume fraction of solid particles.

τ is the effective relaxation given by equation (2):

$$\frac{\mathbf{1}}{\boldsymbol{\tau}} = \frac{\mathbf{1}}{\boldsymbol{\tau_N}} + \frac{\mathbf{1}}{\boldsymbol{\tau_B}} \quad (2)$$

The Néel relaxation time (τ_N) is given by equation (3):

$$\tau_N = \tau_0 e^{\frac{KV_m}{kT}} \quad (3)$$

where τ_0 is on the order of 10^{-9} s, K is the anisotropy constant of the material, V_m the magnetic particle volume, k the Boltzmann constant (1.38 x 10^{23} J/K) and T the temperature (K).

The Brown relaxation time (τ_B) is given by equation (4):

$$\tau_B = \frac{3\eta V_H}{kT} \quad (4)$$

where η denotes the viscosity of the carrier fluid and V_H the hydrodynamic volume of the particle.

χ_0 is the magnetic susceptibility based on Langevin equation, found by equation (5):

$$\chi_o = \frac{\mu_0 m_s^2 \phi V_M}{kT} \times \left(\frac{\coth \xi - \frac{1}{\xi}}{\xi} \right) \tag{5}$$

where m_s denotes the saturation magnetization of the magnetic material,

and finally ξ is the Langevin parameter given by equation (6):

$$\xi = \frac{\mu_0 m_s V H}{kT} \tag{6}$$

For polydispersed nanoparticles, numerical integration over the Gaussian distribution function transforms the SLP (equation 1) to weighted SLP in equation (**7**):

$$\text{weighted SLP} = \int_0^\infty P g(R) dR \tag{7}$$

where $g(R) = \frac{1}{\sqrt{2\pi}\sigma R} e^{\left[\frac{-\left(\ln \frac{R}{R_0}\right)^2}{2\sigma^2}\right]}$ (8a)

and $\int_0^\infty g(R) dR = 1$ (8b)

where ln R_0 is the median and the σ the standard deviation of ln R.

Calculations

As shown in Figure 1-4, the effective relaxation time follows the shortest relaxation time whether it is by Néel or Brown mechanism. To maximize the heat loss, the angular frequency used should match the inverse of the effective relaxation time ($\omega\tau \cong 1$). For 10 nm magnetite nanoparticles, the frequency used should be in the tens of MHz range. Conversely, for particles larger than 10 nm, frequency in the hundreds of kHz to few MHz range should

be sufficient. For the magnetic nanoparticles embedded onto the silica platform, the physical movement and thus the Brown relaxation of the nanoparticles should be rather limited, and the Néel relaxation is expected to be the dominant mechanism of relaxation.

In Figure 1-5, the effect of frequency on the SLP was explored assuming 10 mg/mL of magnetite nanoparticles in water and magnetic field intensity (H) of 10.5 kA/m. The SLP curve shows a distinctive sharp peak in the 10-13 nm size range resulting from the Néel relaxation. Particles above 15 nm exhibit heat loss only by the Brown mechanism, as seen by the hump/tail feature of the SLP curves. Increasing the frequency only increases the SLP where the Néel relaxation is concerned and higher frequencies are needed for smaller nanoparticles.

Figure 1-6 shows how the magnetic field intensity affects the SLP across various particle sizes assuming 10 mg/mL of 11 nm magnetite nanoparticles in water and the frequency of 1 MHz. Increasing the magnetic field intensity very effectively increases the SLP since the SLP is proportional to the square of the magnetic field intensity (equation 1). Unlike the frequency effect, which affects each relaxation mechanism differently, changing the magnetic field intensity affects the SLP uniformly for all particle sizes.

The calculations up to this point were performed with the assumption that the nanoparticles are perfectly monodispersed ($\sigma = 0$), which is impossible to achieve in the real world. To account for polydispersity, the SLP is weighted by the Gaussian distribution function given by equation (8). Figure 1-7 shows the SLP rapidly decreasing as the size distribution increases, thus particles with narrow size distribution are needed to maximize SLP.

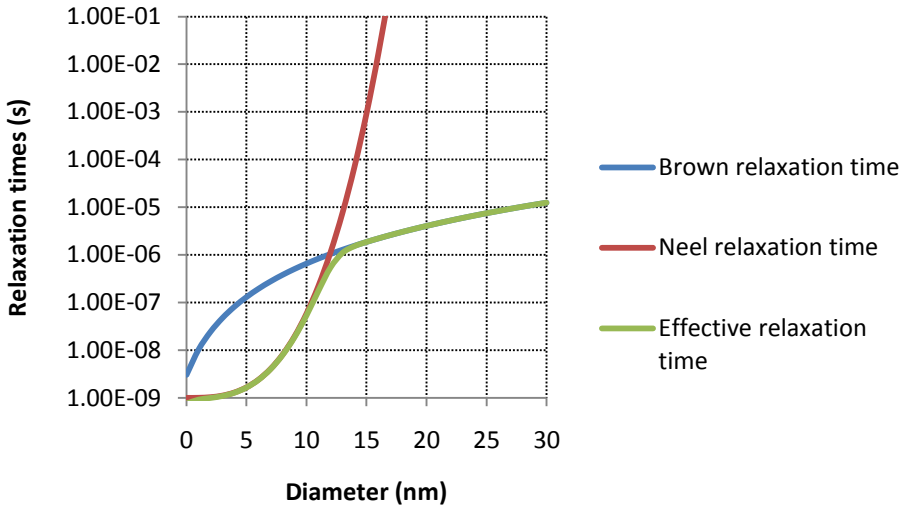

Figure 1-4. Effect of the size of magnetite nanoparticles on the Néel, Brown and effective relaxation time.

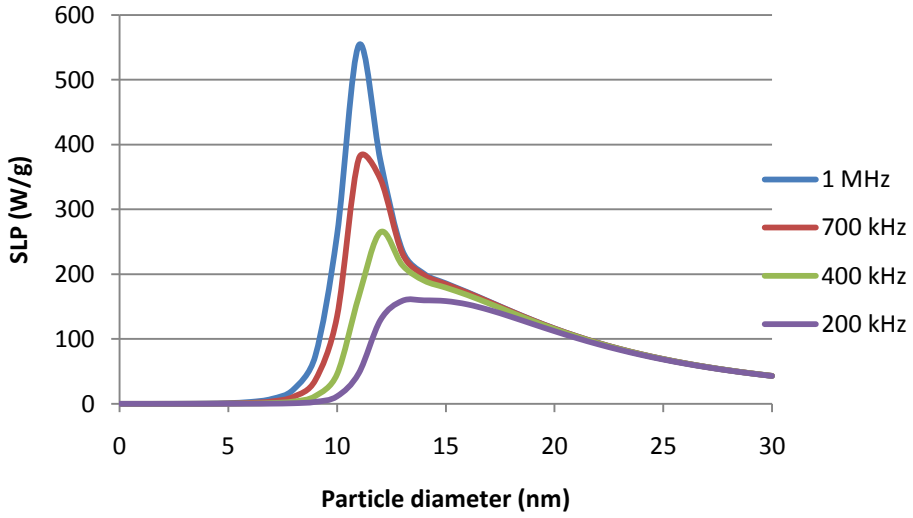

Figure 1-5. Effect of the frequency on the specific loss power (SLP) of 10 mg/mL Fe_3O_4 nanoparticles under 10 kA/m of oscillating magnetic field

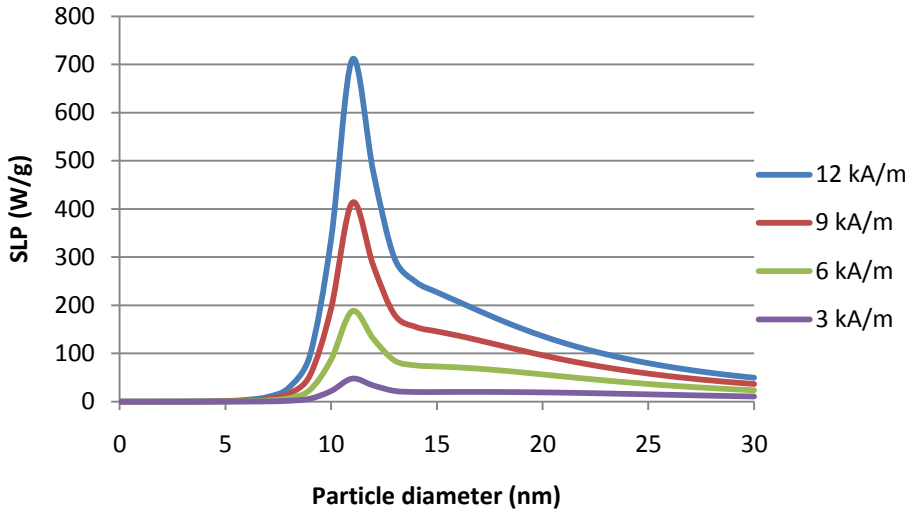

Figure 1-6. Effect of the magnetic field intensity on the SLP of 10 mg/mL Fe_3O_4 nanoparticles under oscillating magnetic field at 1 MHz frequency

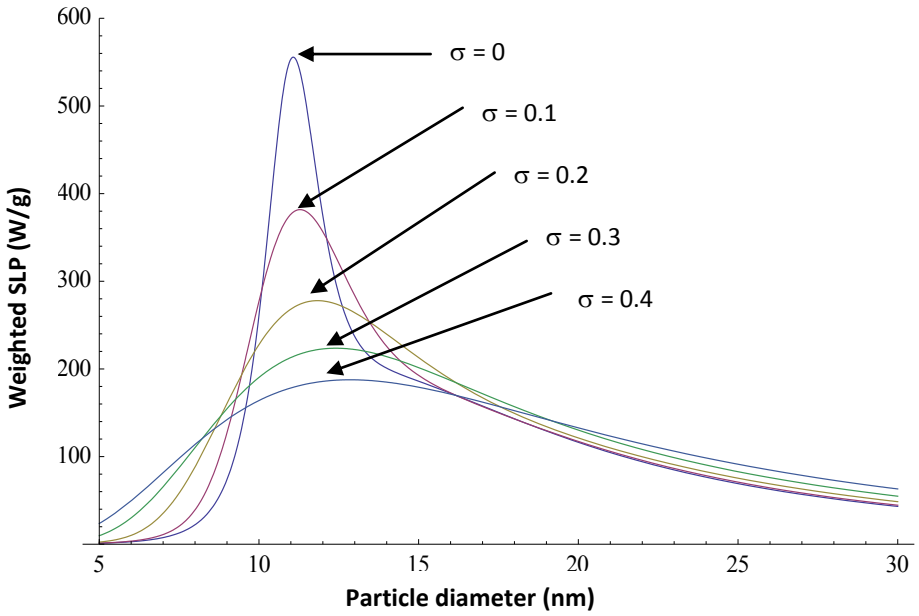

Figure 1-7. Effect of the polydispersity on the SLP of 10 mg/mL Fe_3O_4 nanoparticles at the mean size of 11 nm under 10.5 kA/m oscillating magnetic field at 1 MHz frequency.

Conclusions

In this chapter, the background information on magnetic hyperthermia and its underlying mechanisms were explained. Theoretical calculations allow us to investigate several variables and their influence on the specific heat loss (SLP) of the particles. Increasing the instrumental parameters, i.e. frequency and magnetic field strength, generally increase SLP as well. Effect of the particle size is much more complicated; "resonant" particle size, where the SLP peaks, can be found for each frequency. Size monodispersity of the nanoparticles is also extremely important to the SLP. This theoretical model could be applied to other types of materials, allowing us to tailor our experimental work towards the optimized conditions.

References

(1) Mornet, S.; Vasseur, S.; Grasset, F.; Duguet, E. *Journal of Materials Chemistry* 2004, *14*, 2161-2175.

(2) Gilchrist, R. K.; Medal, R.; Shorey, W. D.; Hanselman, R. C.; Parrott, J. C.; Taylor, C. B. *Annals of Surgery* 1957, *146*, 596-606.

(3) Goya, G. F.; Grazu, V.; Ibarra, M. R. *Current Nanoscience* 2008, *4*, 1-16.

(4) Hergt, R.; Dutz, S.; Müller, R.; Zeisberger, M. *Journal of Physics: Condensed Matter* 2006, *18*, S2919.

(5) Pankhurst, Q. A.; et al. *Journal of Physics D: Applied Physics* 2009, *42*, 224001.

(6) Himmel, M. E.; Ding, S.-Y.; Johnson, D. K.; Adney, W. S.; Nimlos, M. R.; Brady, J. W.; Foust, T. D. *Science (Washington, DC, United States)* 2007, *315*, 804-807.

(7) Merino, S. T.; Cherry, J. *Advances in Biochemical Engineering/Biotechnology* 2007, *108*, 95-120.

(8) Hayes, D. J. *Catalysis Today* 2009, *145*, 138-151.

(9) Ragauskas, A. J.; Williams, C. K.; Davison, B. H.; Britovsek, G.; Cairney, J.; Eckert, C. A.; Frederick, W. J., Jr.; Hallett, J. P.; Leak, D. J.; Liotta, C. L.; Mielenz, J. R.; Murphy, R.; Templer, R.; Tschaplinski, T. *Science (Washington, DC, United States)* 2006, *311*, 484-489.

(10) Moskowitz, B. M. Hitchhiker's Guide to Magnetism: Classes of Magnetic Materials. http://www.irm.umn.edu/hg2m/hg2m_b/hg2m_b.html (accessed Mar 2010).

(11) Hergt, R.; Dutz, S.; Röder, M. *Journal of Physics: Condensed Matter* 2008, *20*, 385214.

(12) Goya, G. F.; Fernandez-Pacheco, R.; Arruebo, M.; Cassinelli, N.; Ibarra, M. R. *Journal of Magnetism and Magnetic Materials* 2007, *316*, 132-135.

(13) Glöckl, G.; et al. *Journal of Physics: Condensed Matter* 2006, *18*, S2935.

(14) Rosensweig, R. E. *Journal of Magnetism and Magnetic Materials* 2002, *252*, 370-374.

(15) Fortin, J.-P.; Wilhelm, C.; Servais, J.; Menager, C.; Bacri, J.-C.; Gazeau, F. *Journal of the American Chemical Society* 2007, *129*, 2628-2635.

CHAPTER 2. SYNTHESIS AND CHARACTERIZATION OF MAGNETIC NANOSTRUCTURES FOR MAGNETIC FLUIDS HYPERTHERMIA

Abstract

This work describes the synthesis and characterization of magnetic nanostructures, based on magnetite (Fe_3O_4), for magnetic hyperthermia effect. First, we report the synthesis of 11 nm spherical Fe_3O_4 nanoparticles, which was determined to be the optimum size for generating heat under oscillating magnetic field (see Chapter 1). The surface of Fe_3O_4 was functionalized with small hydrophilic molecules (i.e. lysine, dopamine), thermo-responsive polymer (PNIPAM), 4-6 nm thick silica layer. Furthermore, Fe_3O_4 nanoparticles were embedded in the framework of mesoporous silica nanoparticles (MSN) with particle size of approximately 100 nm. Lastly, mesoporous Fe_3O_4 nanoparticles with regular particle morphology, approximately 150-200 nm in size, were successfully synthesized.

Introduction

Magnetic hyperthermia is a cancer treatment, administered by heating up magnetic nanoparticles under an oscillating magnetic field. Materials that are suitable for this purpose should be:

- magnetic (i.e. ferromagnetic, ferrimagnetic, or superparamagnetic),
- monodispersed in the submicron size range,
- chemically stable and inert,
- biocompatible.

Metal nanoparticles are desirable because of their high magnetization properties and potential for high magnetic hyperthermia effect.[1] However, metal nanoparticles are easily oxidized in air, their biocompatibility is yet to be proven, and maximizing hysteresis loss is technically difficult. For biological purposes, metal oxides are preferred over their metal counterparts because of their chemical stability and relative ease of surface functionalization, even though their magnetization properties are lower. Of the metal oxides, magnetic iron oxides have emerged as a strong candidate of materials for magnetic hyperthermia because they fulfill all the above requirements and with relatively high magnetization values. In this study, we aim to synthesize monodispersed magnetic iron oxide nanoparticles and functionalize them in different ways for magnetic hyperthermia testing.

The synthesis of magnetite (Fe_3O_4) nanoparticles has been studied extensively in literature. The oldest method to prepare Fe_3O_4 nanoparticles is by co-precipitation of Fe^{2+} and Fe^{3+} salts in aqueous solution at pH 8-14. Even though this method is convenient, the particle size is very difficult to control. To gain better control over the size and shape of the nanoparticles, many alternate methods have been developed including microemulsions, sol-gel, sonochemical reactions, and hydrothermal reactions.[2,3] In this work, we employed high temperature methods, [4,5] which seemed to yield the best results for this the synthesis of Fe_3O_4 nanoparticles in this size range and also can be readily scaled up.[6]

Most non-aqueous methods of Fe_3O_4 nanoparticles synthesis result in hydrophobic particles. Therefore, surface functionalization of the nanoparticles becomes very important in improving the particle dispersibility in water and further conjugation with biologically active moieties. Hydrophilic ligands can be introduced by ligand exchange to increase dispersibility of the nanoparticles in water.[7] The chosen ligands generally have a carboxylate

group or diol that could coordinate with the iron oxide surface and preferably have another hydrophilic functional group for further coupling. A wide variety of organosilanes are also available for surface functionalization. In this study, the surface was functionalized with dopamine, lysine, silica, and poly-*N*-isopropylacrylamide (PNIPAM). PNIPAM is particularly interesting for our applications because it is thermoresponsive and soluble in water at room temperature. At or above its lowest critical solution temperature of 32 ^{o}C, the polymer expels water molecules from its network and becomes hydrophobic.[8]

Our long-term goal involves immobilization of catalytic groups onto a solid magnetic support, thus embedding Fe_3O_4 onto the mesoporous silica support could be beneficial in various ways. Mesoporous silica nanoparticles (MSN) have high surface area (around 1,000 m^2/g compared to less than 50 m^2/g of the Fe_3O_4), tunable particle size, morphology,[9] pore size and pore structure.[10] MSNs can be functionalized with various organic or inorganic groups by co-condensation or post-synthesis grafting with silane derivatives.[11-13] Additionally, MSNs have been proven to be efficient support for immobilization of catalysts.[14]

Lastly, in an attempt to take advantage of mesoporous structure while having a high Fe loading, mesoporous Fe_3O_4 was synthesized. To the best of our knowledge, the effect of oscillating magnetic field on mesoporous Fe_3O_4 nanoparticles have not yet been reported, thus this material would be very interesting to investigate. Mesoporous Fe_3O_4 was first reported in 2006 by Jiao and co workers using KIT-6 type mesoporous silica as template.[15] While the researchers achieved great pore structures, no mention was made about the overall particle size or morphology, which is very important for our application. In this report, we

applied the nanocasting technique to MCM-48 template[10] to synthesize mesoporous Fe_3O_4 nanoparticles with well-defined size and shape.

Materials and methods

All reagents were purchased from commercial sources and used as received without further purification.

1. Monodispersed magnetite (Fe_3O_4) nanoparticles

11 nm Iron oxide nanoparticles (IO11)

11 nm Fe_3O_4 nanoparticles were synthesized by thermal decomposition of iron oleate precursor according to literature procedure.[6,16] Iron oleate complex (IOl) was synthesized by stirring 10.8 g $FeCl_3 \cdot 6H_2O$ (40 mmol) with 36.5 g sodium oleate (120 mmol) in a mixture of water/ethanol/hexane (4:3:7 by volume) at 70 ^oC for 4 hours under argon flow. After cooling to room temperature, the water layer was removed in a separation funnel and the organic layer was washed with water 3 times. Hexane was evaporated by rotary evaporation and the resulting product was dried under high vacuum at 35 ^oC for 18 hours.

The IOl was used as a precursor for the synthesis of Fe_3O_4 nanoparticles. Typically, 11 nm Fe_3O_4 nanoparticles was synthesized by heating 3.6 g IOl (4 mmol) with 0.57 g oleic acid (2 mmol) and 20 g 1-octadecene to 320 ^oC (heating rate 3.3 ^oC/min) and refluxing for 30 minutes. After cooling to room temperature, the precipitates were collected by centrifugation, washed extensively with ethanol and lyophilized overnight. Nanoparticles of different sizes could also be synthesized by varying the ratio between IOl and oleic acid or changing the reflux temperature.

Surface functionalization of Fe_3O_4 nanoparticles

A typical ligand exchange process with lysine (Lys-IO11) or dopamine (Dop-IO11) was achieved by stirring 600 mg of the as-synthesized nanoparticles with 3.0 mmol of the ligand in 40 mL 1,2-dichlorobenzene and 40 mL dimethylsulfoxide overnight. The material was washed 3 times with ethanol.

Silica-coated iron oxide nanoparticles (SiO_2-IO11)

100 mg Lys-IO11 was mechanically stirred at room temperature in a solution of 28 wt% NH_4OH/water/ethanol (1:10:30 by volume). A solution of 90 mg of TEOS in 20 mL ethanol was added dropwise over 10 minutes. After 12 hours of stirring, the material was magnetically decanted and washed several times with water and ethanol.

2. PNIPAM-iron oxide-composite (PNIPAM-IO)

PNIPAM-Fe_3O_4 nanoparticles were synthesized according to the literature procedure.[17] First, iron oxide nanoparticles were synthesized by co-precipitation method. 4.1 g $FeCl_3 \cdot 6H_2O$ (15 mmol) and 2.3 g $FeSO_4 \cdot 7H_2O$ (8.5 mmol) were stirred at room temperature under argon in 100 mL water. After an hour, 22.4 mL of 28% w/w NH_4OH was rapidly injected into the solution, which turned black immediately. The mixture was heated to 80 ^oC over 3 hours, then 1 mL of oleic acid was added over 1 hour to form a double layer of oleate coatings over the particles. After cooling to room temperature, 100 mL of toluene was added to the mixture in a separatory funnel. Small amount of NaCl was added to extract iron oxide nanoparticles into the toluene layer. Once the organic layer turned dark brown, the water layer was removed. The toluene layer was washed 3 times with water and NaCl. The iron

oxide solution was then refluxed under argon overnight. The content was diluted to 100 mg/mL with toluene and kept in a stoppered round-bottom flask.

The iron oxide surface was functionalized with methacryloxysilane by adding 100 μL of 3-(trimethoxysilyl)propylmethacrylate (MAPS, 420 μmol), 279 uL of triethylamine (2 mmol) and 100 mL toluene to 5 mL of 100 mg/mL iron oxide solution. The mixture was stirred at room temperature in argon for 24 hours. The MAPS-IO was precipitated by adding ethylether and collected by centrifugation, then washed 5 times with ethyl ether and lyophilized overnight.

Polymerization of *N*-isopropylacrylamide (NIPAM) was done by stirring 100 mg MAPS-IO with 100 mL acetone, 51 mg Azobisisobutyronitrile (AIBN, 0.3 mmol), 2.5 g NIPAM and 100 mL water was stirred at room temperature under argon for 10 minutes. The solution was slowly heated to 70 ^{o}C and stirred under argon for 6 hours. The product was magnetically separated and washed 5 times with water.

3. Iron oxide-embedded mesoporous silica nanoparticles (IO-MSN)

Fe_3O_4 nanoparticles were embedded in the mesoporous silica framework by co-condensation method that was developed in our lab. Briefly, 200 mg Lys-IO11 were sonicated in 2 mL water to disperse the particles. 0.5 g CTAB was mechanically stirred in 235 mL water and 1.8 mL of 2.0 M sodium hydroxide. The solution was slowly heated up. At 75 ^{o}C, the Fe_3O_4 nanoparticles mixture was rapidly injected into the solution and rinsed with 3 mL water. At 80 ^{o}C, 2.5 mL of tetraethylorthosilicate (TEOS) was injected dropwise into the mixture. After 2 hours of stirring at 80 ^{o}C, the precipitate was filtered and washed

extensively with water and methanol. The surfactant was removed by calcination at 350 ^{o}C for 6 hours.

4. *Mesoporous iron oxide nanoparticles (MIO)*

MCM-48 template

To prepare the mesoporous iron oxides, we first synthesized a MCM-48 type mesoporous silica material as the structure-directing template. 1.0 g CTAB and 4.0 g of Pluronic F127 ($EO_{106}PO_{70}EO_{106}$) were mixed in 298 mL of water/ammonia/ethanol solution (2.8 wt% ammonia/ethanol) 2.5/1 (v/v)). Then, 3.6 g TEOS was added into the solution at room temperature. After vigorous stirring for 1 min, the reaction mixture was kept under static conditions for 1 day at room temperature for the complete condensation of silica.

The resulting solid MSN product was isolated by centrifugation and washed with copious amount of water. The product was hydrothermally treated at 150 ^{o}C in a Teflon-lined autoclave for 48 hours to enlarge the pore size. The resulting product was isolated by centrifugation and dried in air overnight. The product was dried at 37 ^{o}C for 2 hours and calcined at 550 ^{o}C for 6 hours to remove the surfactant.

Impregnation and template removal

$Fe(NO_3)_3$ was used as the iron precursor. Impregnation was carried out by mixing a very concentrated ethanolic solution of precursor (120% of the sample pore volume) with the sample, drying at 60 ^{o}C for 2 hours then calcining the sample at 350 ^{o}C for 5 hours. The process was repeated 3-5 times to fill the pore channels. The final product was calcined at 550 ^{o}C for 5 hours. The silica template was then removed by mixing the sample with 2 M

NaOH overnight. Product was collected by centrifugation and washed with copious amount of water.

Reduction with hydrogen gas

Structural transformation of α-Fe_2O_3 to Fe_3O_4 type iron oxide was accomplished by reduction under H_2 flow at 300 ^oC for 5 hours.

Results and discussion

1. ***Monodispersed 11 nm iron oxide nanoparticles (IO11)***

Monodispersed 11 nm Fe_3O_4 nanoparticles was synthesized by high-temperature decomposition of iron oleate.[6] The TEM micrograph (Figure 2-1a) shows nanoparticles of 11 nm with uniform particle size. The X-ray diffraction pattern of the nanoparticles confirms the presence of crystalline Fe_3O_4 (Figure 2-1b). The field-dependent magnetization curve of the nanoparticles measured at 300 K (Figure 2-1c) exhibits no hysteresis, meaning they are superparamagnetic. The saturation magnetization value of the nanoparticles is approximately 48 emu/g. It is worth noting that we are not limited only to particles of this size; we focus on 11 nm because it is theoretically optimized for heating under an oscillating magnetic field. The size of the nanoparticles can be manipulated by the concentration of reagents, reaction time, temperature and solvent (results not shown).

The surface of the as-synthesized Fe_3O_4 nanoparticles is covered with oleic acid at 11% by weight of the material, as shown by the TGA curve (Figure 2-1d, solid green line). After the surface ligand exchange process, the ligands dopamine and lysine account for over 30% by weight of the material (Figure 2-1d, dashed blue line and dotted red line).

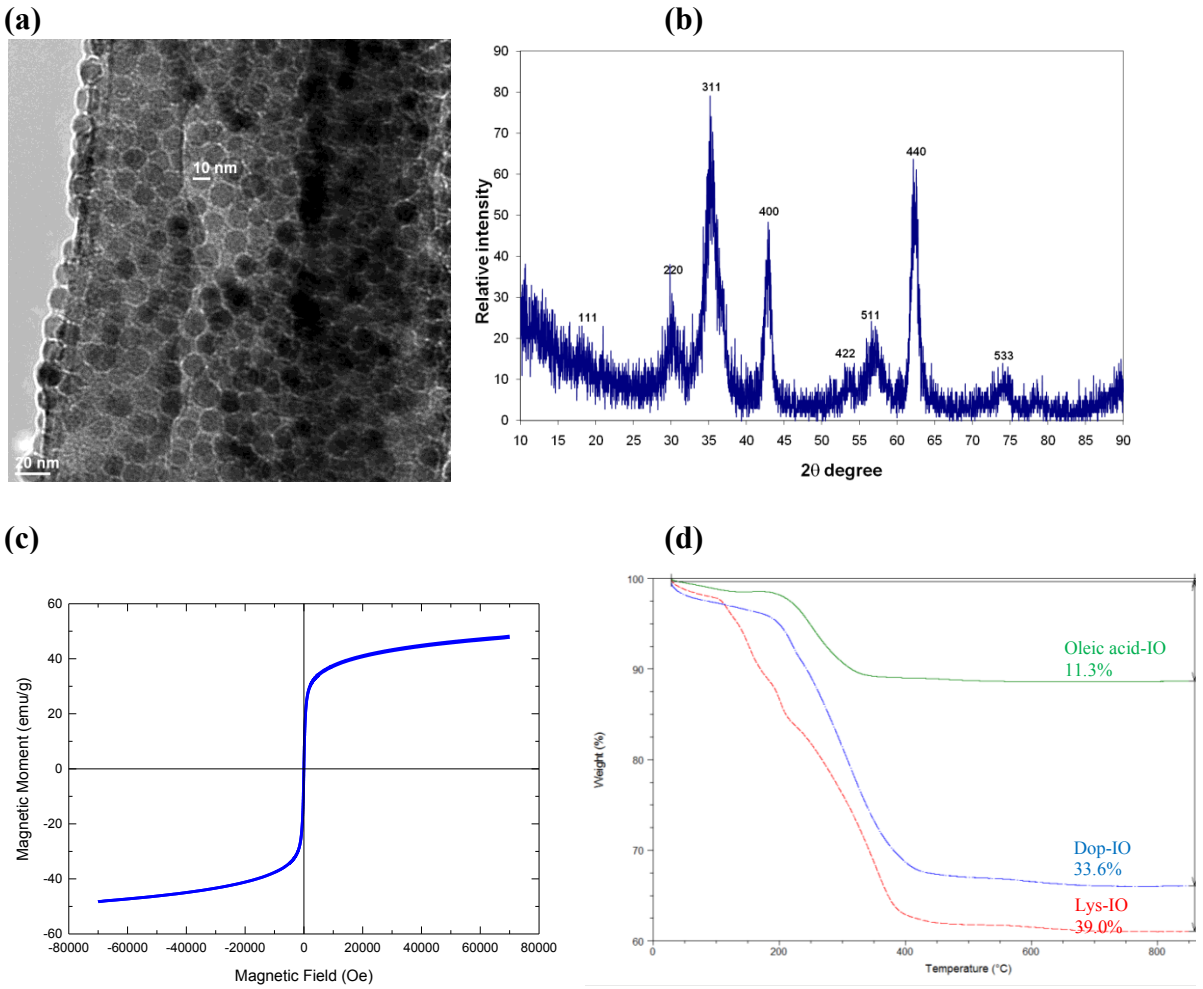

Figure 2-1 (a) TEM micrograph, (b) X-ray diffraction pattern, and (c) magnetization versus applied magnetic field at 300 K of as-synthesized monodispersed 11 nm Fe_3O_4 nanoparticles. (d) TGA curves of the nanoparticles 11 nm Fe_3O_4 nanoparticles, coated with oleic acid (solid green line), dopamine (dashed blue line) and lysine (dotted red line).

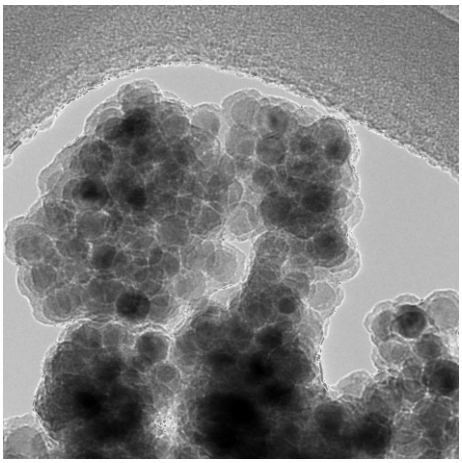

Figure 2-2. TEM micrograph of silica-coated iron oxide nanoparticles.

Aside from the small hydrophobic ligands, the surface of the Fe_3O_4 nanoparticles could also be coated with silica layer. The thickness of the layer can be tuned by varying the amount of precursors. Figure 2-2 shows a silica layer of 4-6 nm around the 11 nm Fe_3O_4 nanoparticles.

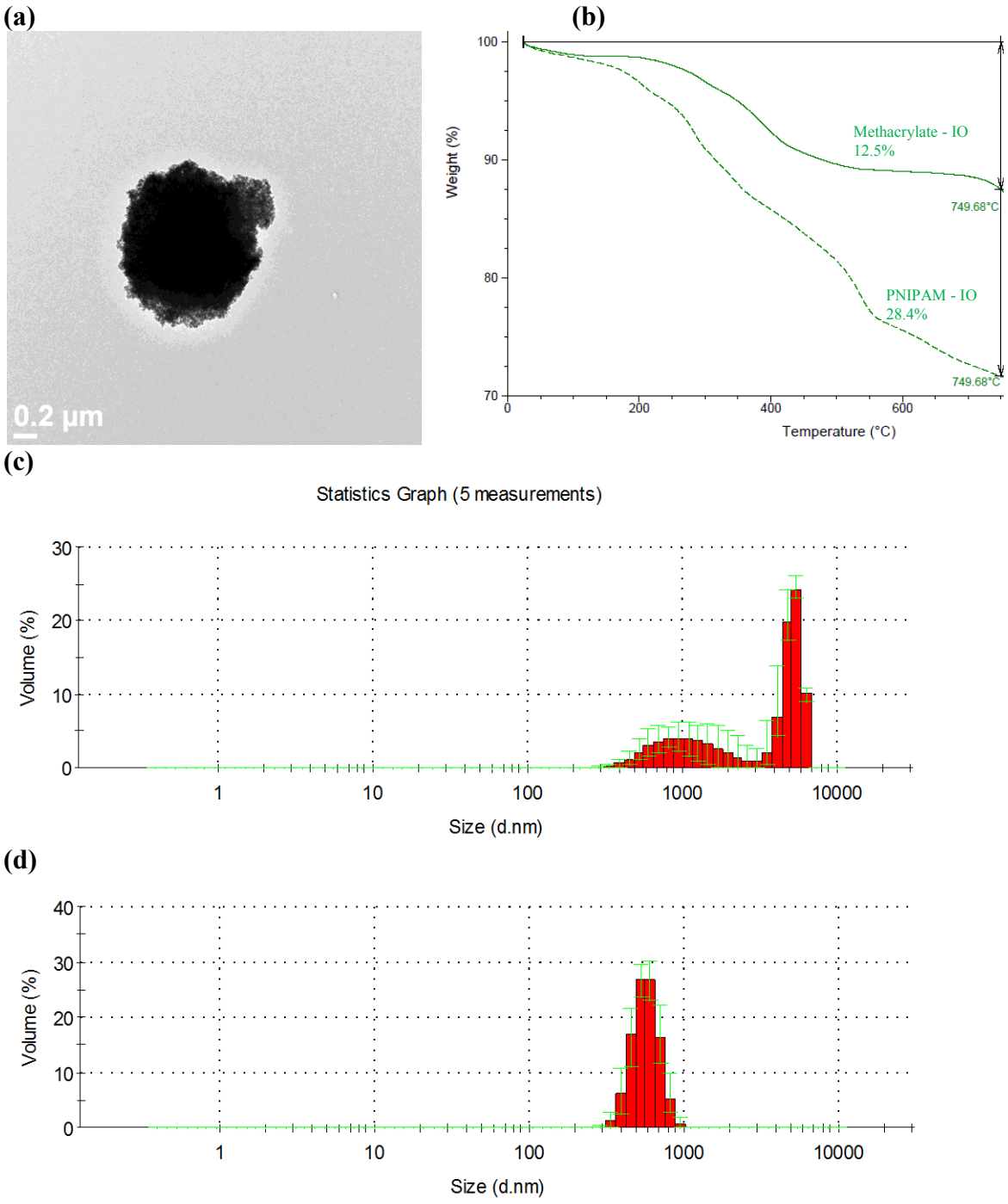

Figure 2-3. (a) TEM micrograph of PNIPAM-coated iron oxide nanoparticles, (b) TGA curves of the iron oxide nanoparticles before (solid line) and after (dotted line) polymerization, and the particle size distribution by DLS of PNIPAM-IO at (c) 25 ^{o}C and (d) 40 ^{o}C.

2. *PNIPAM-coated iron oxide (PNIPAM-IO)*

The Fe_3O_4 nanoparticles were synthesized by the co-precipitation method followed by grafting of methacryloxy silane for further coupling with the *N*-isopropylacrylamide. Following the radical polymerization of PNIPAM, the polymer weight was 28.4% of the material (TGA, Figure 2-3b). This method of polymerization produces micron-size composites of particles, as seen in the TEM micrograph (Figure 2-3a) and the size distribution by dynamic light scattering (DLS, Figure 2-3c) of the material. The material exhibits proper thermoresponsive properties above the LCST (32 ^{o}C): the composites agglomerate at 40 ^{o}C (Figure 2-3d) compared to at room temperature (Figure 2-3c).

3. *Iron oxide-embedded MSN (IO11-MSN)*

The 11 nm Fe_3O_4 nanoparticles were incorporated into the mesoporous silica framework during the co-condensation process. This method resulted in MCM-41 type mesoporous structure (Figure 2-4c, low-angle XRD) with uniform spherical nanoparticles of 110 nm (Figure 2-4a, SEM) and BET surface area of 858.5 m^2/g. The material exhibit type IV N_2 sorption isotherms (Figure 2-4f), which is typical of MCM-41, with average BJH pore size of 2.8 nm. TEM micrograph of the material (Figure 2-4b) reveals the presence of Fe_3O_4 nanoparticles embedded inside the MSN framework, which is further confirmed by the high-angle XRD (Figure 2-4d). The material is superparamagnetic, as demonstrated by the absence of hysteresis in the magnetization curve (Figure 2-4g), with the saturation magnetization value of approximately 10 emu/g.

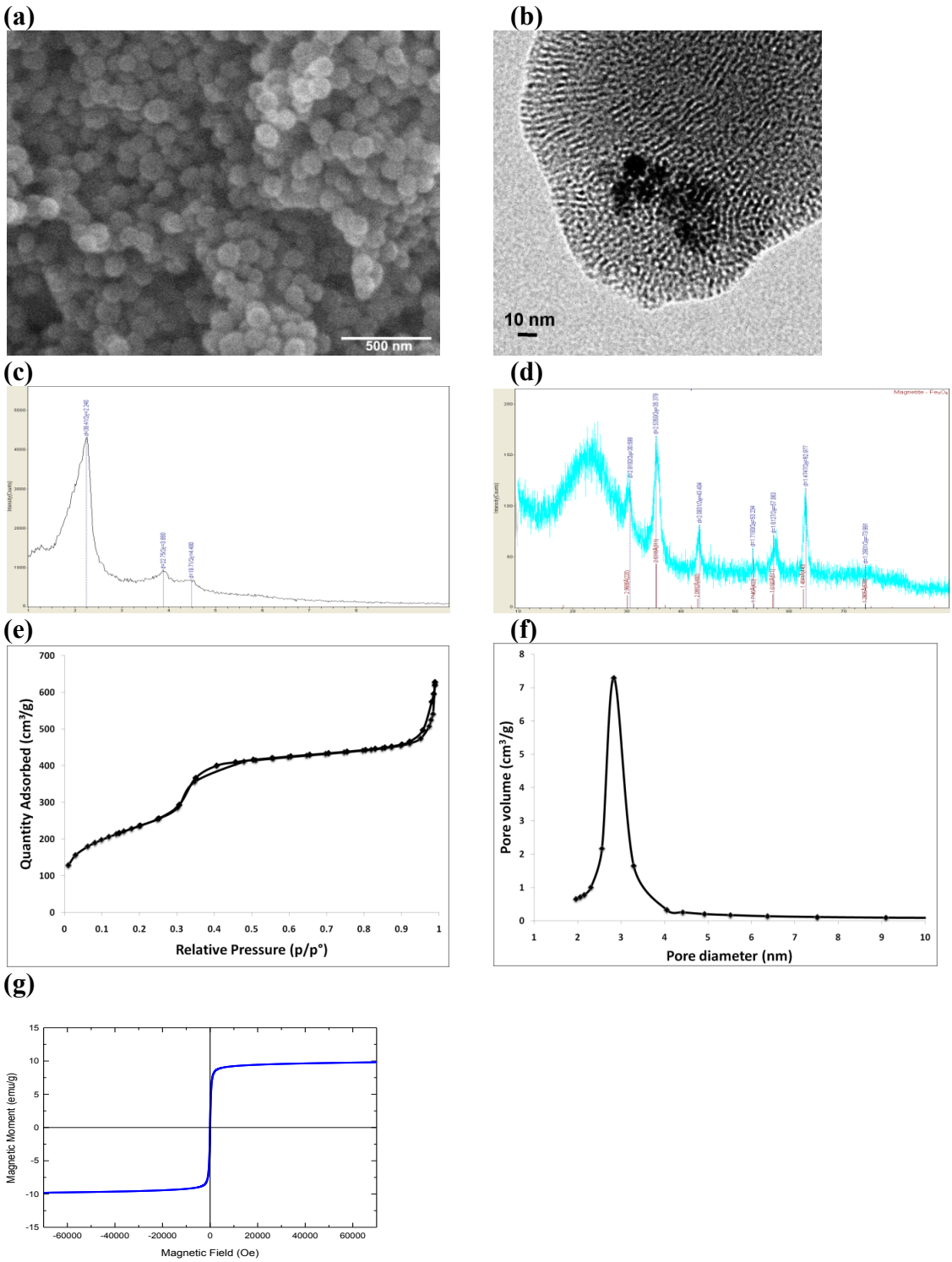

Figure 2-4. (a) SEM and (b) TEM micrographs, (c) low-angle and (d) high-angle powder X-ray diffraction patterns, (e) N_2 sorption isotherms, (f) BJH pore size distribution, and (g) magnetization versus applied magnetic field at 300 K of Fe_3O_4 embedded mesoporous silica nanoparticles (IO11-MSN)

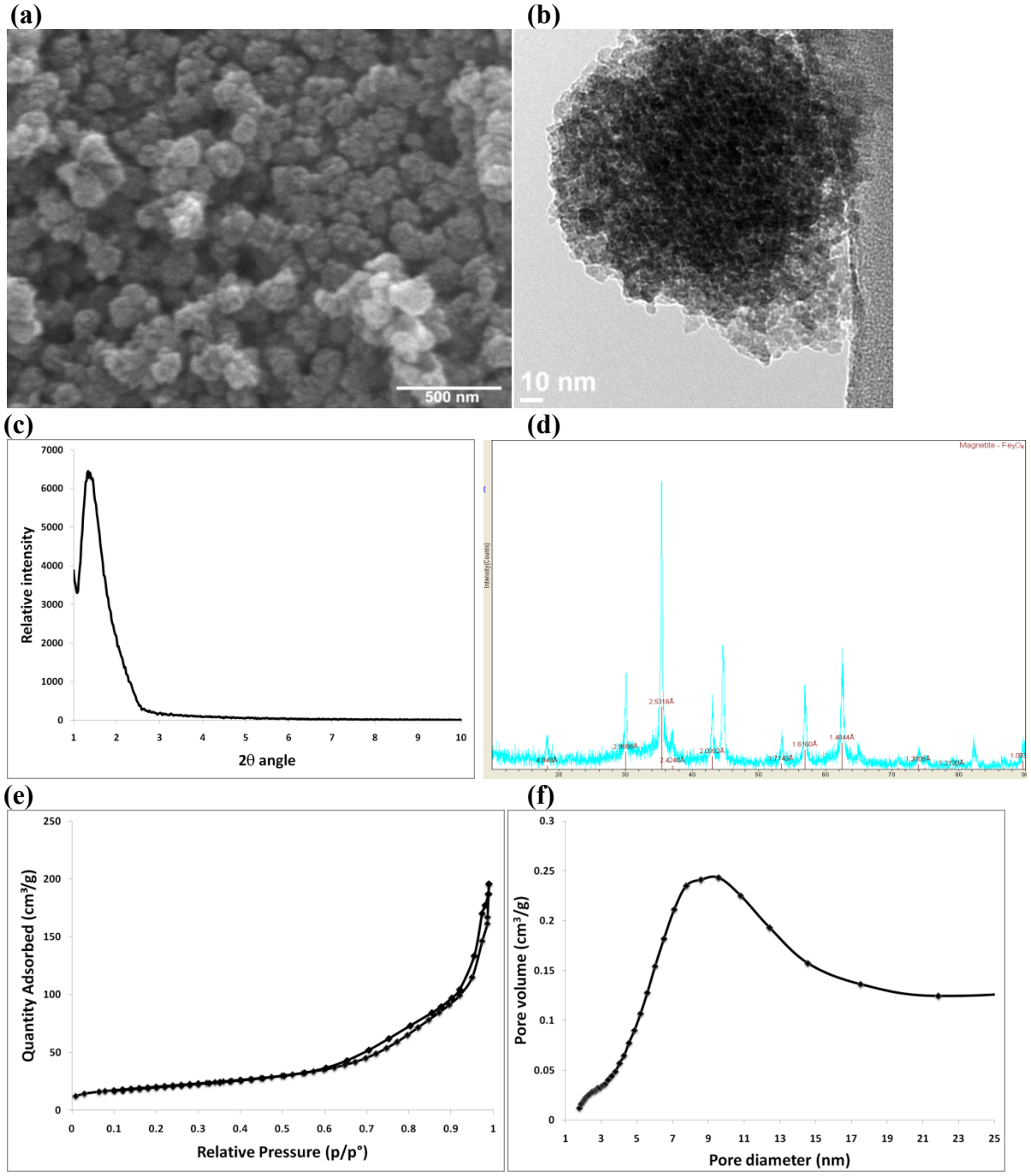

Figure 2-5. (a) SEM and (b) TEM micrographs, (c) low-angle and (d) high-angle powder X-ray diffraction patterns, (e) N_2 sorption isotherms, and (f) BJH pore size distribution of mesoporous Fe_3O_4 nanoparticles (MIO)

4. Mesoporous iron oxide nanoparticles (MIO)

Mesoporous Fe_3O_4 nanoparticles were synthesized by nanocasting method, using MCM-48 type material as template. The resulting material have relatively uniform spherical shape as shown in the SEM and TEM micrographs (Figure 2-5a,b). The material exhibits mesostructures, as evidenced in the sorption isotherms (Figure 2-5e), with the BET surface area of 72.7 m^2/g and BJH average pore size of 8.6 nm (Figure 2-5f). However, only the *100* peak of tetragonal *I*41/*a* mesoporous structure, which is the typical replication structure of the cubic *Ia*-3*d* MCM-48 template, is observed (low-angle XRD, Figure 2-5c) indicating that the pore structures are not very regular. The high-angle XRD (Figure 2-5d) confirms the Fe_3O_4 phase in the particles.

Conclusions

In this work, we explored several variations of magnetic Fe_3O_4 nanoparticles for applications in magnetic hyperthermia. The synthesis and characterization of the following materials of interest were reported:

- 11 nm iron oxide (IO11) nanoparticles (optimized size of magnetite for hyperthermia)
    - with dopamine or lysine coating (hydrophilic and allows for further functionalization)
    - with silica coating (hydrophilic, allows for further functionalization and can affect Brownian motion in the oscillating magnetic field)
    - with PNIPAM coating (thermoresponsive)
- IO11 embedded mesoporous silica nanoparticles (support for catalysis with minimum Fe loading)

- mesoporous iron oxide nanoparticles (support for catalysis with maximum Fe loading)

While this work was tailored towards applications under oscillating magnetic field, the materials and lessons learned from the synthesis of these materials will certainly be useful for a variety of applications for our future work.

References

(1) Hergt, R.; Dutz, S.; Röder, M. *Journal of Physics: Condensed Matter* **2008**, *20*, 385214.

(2) Gupta, A. K.; Gupta, M. *Biomaterials* **2005**, *26*, 3995-4021.

(3) Laurent, S.; Forge, D.; Port, M.; Roch, A.; Robic, C.; Vander Elst, L.; Muller, R. N. *Chemical Reviews (Washington, DC, United States)* **2008**, *108*, 2064-2110.

(4) Hyeon, T.; Lee, S. S.; Park, J.; Chung, Y.; Na, H. B. *Journal of the American Chemical Society* **2001**, *123*, 12798-12801.

(5) Sun, S.; Zeng, H. *Journal of the American Chemical Society* **2002**, *124*, 8204-8205.

(6) Park, J.; An, K.; Hwang, Y.; Park, J.-G.; Noh, H.-J.; Kim, J.-Y.; Park, J.-H.; Hwang, N.-M.; Hyeon, T. *Nature Materials* **2004**, *3*, 891-895.

(7) Lattuada, M.; Hatton, T. A. *Langmuir* **2006**, *23*, 2158-2168.

(8) Ono, Y.; Shikata, T. *Journal of the American Chemical Society* **2006**, *128*, 10030-10031.

(9) Trewyn, B. G.; Whitman, C. M.; Lin, V. S. Y. *Nano Letters* **2004**, *4*, 2139-2143.

(10) Kim, T.-W.; Chung, P.-W.; Slowing, I. I.; Tsunoda, M.; Yeung, E. S.; Lin, V. S. Y. *Nano Letters* **2008**, *8*, 3724-3727.

(11) Chen, H.-T.; Huh, S.; Lin, V. S. Y. *Catalyst Preparation* **2007**, 45-73.

(12) Slowing, I. I.; Trewyn, B. G.; Giri, S.; Lin, V. S. Y. *Advanced Functional Materials* **2007**, *17*, 1225-1236.

(13) Trewyn, B. G.; Slowing, I. I.; Giri, S.; Chen, H.-T.; Lin, V. S. Y. *Accounts of Chemical Research* **2007**, *40*, 846-853.

(14) Huh, S.; Chen, H.-T.; Wiench, J. W.; Pruski, M.; Lin, V. S. Y. *Angewandte Chemie, International Edition* **2005**, *44*, 1826-1830.

(15) Jiao, F.; Jumas, J.-C.; Womes, M.; Chadwick, A. V.; Harrison, A.; Bruce, P. G. *Journal of the American Chemical Society* **2006**, *128*, 12905-12909.

(16) Bronstein, L. M.; Huang, X.; Retrum, J.; Schmucker, A.; Pink, M.; Stein, B. D.; Dragnea, B. *Chemistry of Materials* **2007**, *19*, 3624-3632.

(17) Sun, Y.; Ding, X.; Zheng, Z.; Cheng, X.; Hu, X.; Peng, Y. *Chemical Communications (Cambridge, United Kingdom)* **2006**, 2765-2767.

CHAPTER 3. TEMPERATURE RESPONSE OF MAGNEIC NANOPARTICLES UNDER OSCILLATING MAGNETIC FIELD AND THEIR APPLICATIONS FOR CHEMICAL REACTIONS

Abstract

In this study, we set out to evaluate some magnetic materials, both from commercial sources and synthesized in-house, for use as heat source under oscillating magnetic field. Changing surface coating has a profound effect on the SLP of the materials. Under our conditions, the materials that clustered e.g. silica-coated and PNIPAM-coated iron oxides exhibited the highest heat generation, while iron oxides embedded in MSNs and mesoporous iron oxides did not perform as well. We also investigated the effects of this heat for the synthesis of 7-hydroxycoumarin-3-carboxylic acid. Application of oscillating magnetic field systems to the uncatalyzed synthesis of the coumarin derivative effectively increased the reaction rate compared to the room temperature control.

Introduction

In an oscillating magnetic field system, the magnetic nanoparticles act as a local "hot-spot" to heat up the surrounding environment by hysteresis loss or relaxation mechanisms.[1] In this study, the heating efficiency of the nanoparticles termed Specific Loss Power (SLP), of various magnetic materials from Chapter 2 are tested under oscillating magnetic field. The SLP depends on various factors including the type, size and coating of the material. The SLP of magnetic nanoparticles are typically reported under the conditions physiologically suitable for hyperthermia therapy, which limits the product of magnetic field and frequency

($H \cdot f$) to $4.85 \times 10^8 \frac{A}{m \cdot s}$.[2] Since hyperthermia in human patients is not the eventual goal of this project, the conditions evaluated in this study are not restricted by this $H \cdot f$ limit.

7-Hydroxycoumarin-3-carboxylic acid is a blue fluorophore with functional carboxylic group that can be used for coupling with sugars,[3,4] proteins[5] and nucleic acids.[6,7] The fluorescence of this compound allows for convenient quantification and potential use as labeling agents for any future *in vivo* applications. 3-Carboxycoumarins can be conveniently and efficiently synthesized at room temperature in water[8] from 2-hydroxybenzaldehydes and Meldrum's acid with acetate catalyst,[9] or at high temperature without a catalyst.[10] 7-Hydroxycoumarin-3-carboxylic acid can be similarly synthesized from 2,4-dihydroxybenzaldehyde and the reaction is promoted by ultrasound irradiation.[11]

Aside from hyperthermia therapy, thermal energy from magnetic nanoparticles under an oscillating magnetic field shows promise in controlled-release drug delivery applications. However, most of these controlled-release mechanisms are based on physical changes e.g. phase transition of lipid bilayers,[12,13] conformational changes of thermoresponsive polymers,[14,15] and strand separation of DNA base pairs.[16] To date, there is only one example of this energy being utilized for causing chemical changes i.e. thermal degradation of hydrogels.[17] In this chapter, we report a preliminary study on the application of the oscillating magnetic field system to the uncatalyzed synthesis of the fluorescent dye 7-hydroxycoumarin-3-carboxylic acid.

Materials and methods

The magnetic nanoparticles are all synthesized in-house as described in Chapter 2 of this thesis, with the exception of the 10-30 nm Fe/FeO and 5-15 nm Co/Co_3O_4 nanoparticles,

which were purchased from Alfa Aesar. All other chemical reagents are used as purchased from Aldrich, unless stated otherwise.

All measurements in the oscillating magnetic field were carried out in a custom-made instrument, built by R. Vincent of ROV NMR probes (Figure 3-1). The instrument is fitted with a coil with the following parameters: inner diameter = 13 mm, length = 32 mm, inductance = 25 μH, number of turns = 70, copper wire diameter = 0.4 mm, and quality factor ≅ 50. The frequency generated from this device is tunable from 50 kHz to 2 MHz and the magnetic field intensity is adjustable for up to 12 kA/m. The temperature of the coil is regulated by circulating lamp oil, whose temperature is stabilized through a water-cooled heat exchanger.

Calibration and SLP of nanoparticles in oscillating magnetic field:

For calibration tests, 300 μL of water or any other desired liquid was transferred to a 3" NMR tube (shortened from standard NMR tubes). For SLP evaluation of 10 mg/mL suspensions, 3 mg of the nanoparticles were dispersed in 300 μL of water in the sample tube by vortexing and brief sonication. The sample tube was insulated by a custom-made 1 mm-thick Teflon jacket, and inserted into the heating coil so that bottom of the tube is positioned at the center of the coil. The temperature of the solution was monitored *in situ* using a fiberoptic thermoprobe (Omega) which does not interfere with the magnetic field. The normalized temperature rise was calculated by subtracting the background temperature of the circulating oil from the solution temperature under oscillating magnetic field.

Synthesis of 7-hydroxycoumarin-3-carboxylic acid in oscillating magnetic field:

27.8 mg (200 μmol) 2,4-dihydroxybenzaldehyde was dissolved in 10 mL of 0.083 M pyrophosphate buffer, pH 8.7. 20 mM of 2,2,-dimethyl-1,3,-dioxane-4,6-dione (Meldrum's acid) in pyrophosphate buffer was similarly prepared. The solutions of the reagents were always made fresh before every reaction as the reagents could undergo decomposition after several hours in solution. For a typical reaction, 3 mg of nanoparticles were placed in the sample tube and 150 μL of each solution was transferred into the sample tube using micropipettes. Then, the mixture was dispersed by vortexing and brief sonication. The reaction vial was placed in the coil of the oscillating magnetic field instrument, similarly to the calibration tests, under the desired frequency and field strength. The control reaction was performed at room temperature or warmed with an oil bath to the temperature of the bulk solution under oscillating magnetic field. After one hour, the reaction mixture was centrifuged at 14,000 rpm for 5 mins. Then, 20 μL of the supernatant was diluted to 4 mL with pyrophosphate buffer. The fluorescence of the solution was measured at 445 nm after excitation at 386 nm, using a fluorometer (Fluoromax-2®). Concentration of the product was determined by comparing the fluorescence intensity with the standard calibration curve (Figure S1).

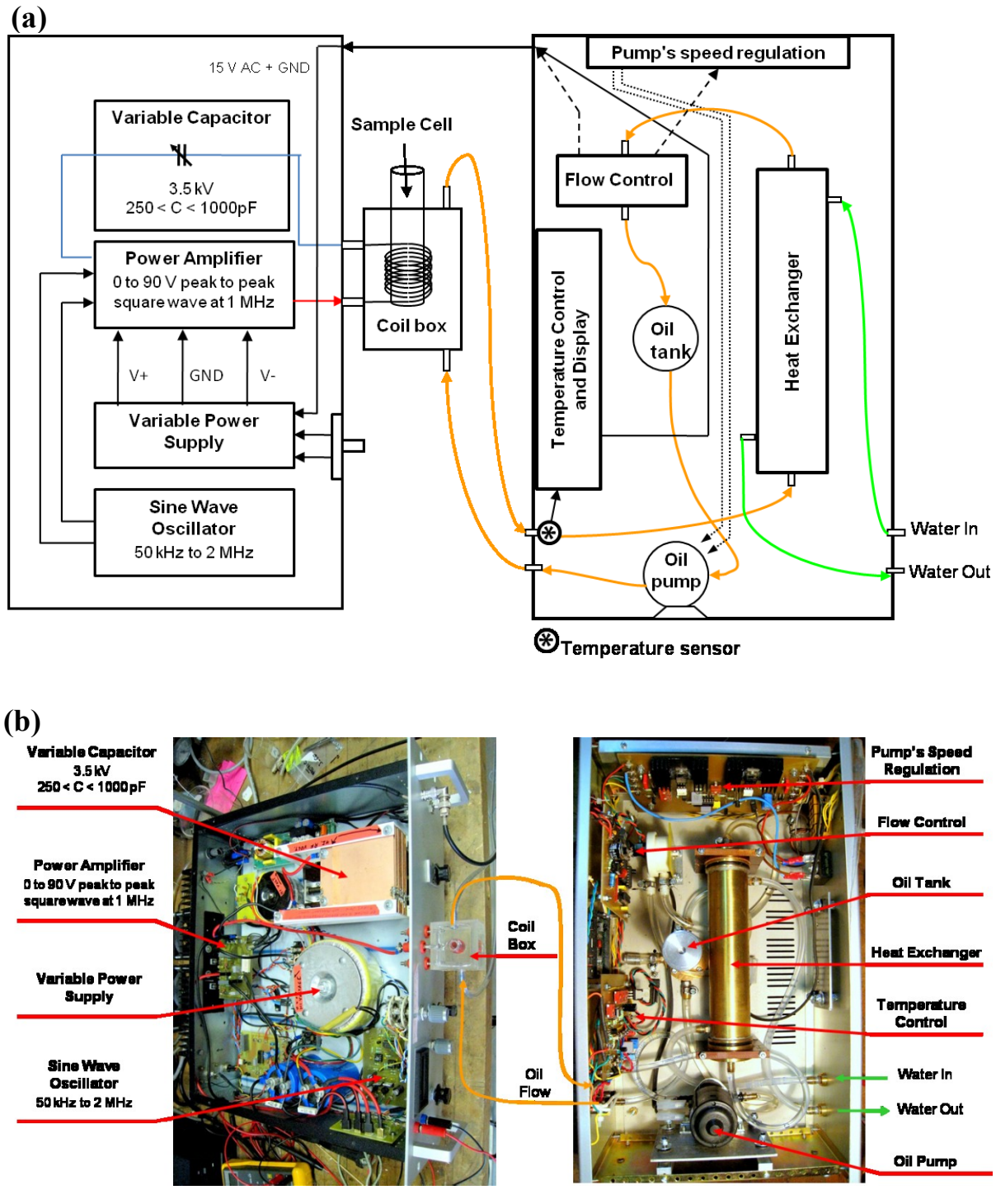

Figure 3-1 Schematic diagram (a) and photographs (b) of main components of the magnetic oscillating magnetic field generator. The sine wave oscillator and amplifier are depicted on the left side of the figure, the coil and sample holder are located in the center, and the cooling system is shown on the right.

Results and discussion

Calibration of the oscillating magnetic field Instrument

To assess the heating effect generated from the magnetic nanoparticles, several measures were taken into account for background heating. First, the coil box was especially engineered to have circulating oil to regulate the native coil heating from passing the current. An insulating Teflon jacket was also used to keep the heat generated in the solution from the influence of the coil heating and the cooling speed. Moreover, the sample was positioned so that the bottom of the vial is aligned with the center of the coil to maximize the hyperthermia effect. Lastly, to ensure that the measured temperature rise of the solution results purely from the magnetic hyperthermia effect, background heating of water inside the oscillating field was investigated. As shown in Figure 3-2, the temperature of the water (blue line) matches very well with the temperature of the circulating oil (red line). Thus, the temperature rise of a magnetic fluid could be normalized by subtracting the temperature of the circulating oil (background) from the final temperature of the solution.

Effect of coating: lysine, dopamine, and silica

As shown in Figure 3-3, the rate of temperature rise of lysine-coated 11 nm iron oxide nanoparticles (Lys-IO11, 7.8 ^{o}C/min) was in excellent agreement with the theoretical prediction for 10 mg/mL of 11 nm Fe_3O_4 nanoparticles (7.9 ^{o}C/min), assuming 1 nm-thick coating, 1 MHz frequency and 10.5 kA/m magnetic field. Encouraged by this result, other coatings of the same core material were tested under the same conditions. As shown in Figure 3-4, dopamine seemed to reduce the SLP of the Fe_3O_4 nanoparticles, while silica coating enhanced the effect. Since the 4-6 nm silica layer was much thicker than the small

molecule of dopamine or lysine coating, in theory this should result in a smaller increase in temperature. We suspect that the increased dispersibility of the material in water could explain the difference between Lys-IO11 and Dop-IO11. On the other hand, clustering might also play a crucial role (see effect of PNIPAM coating below).

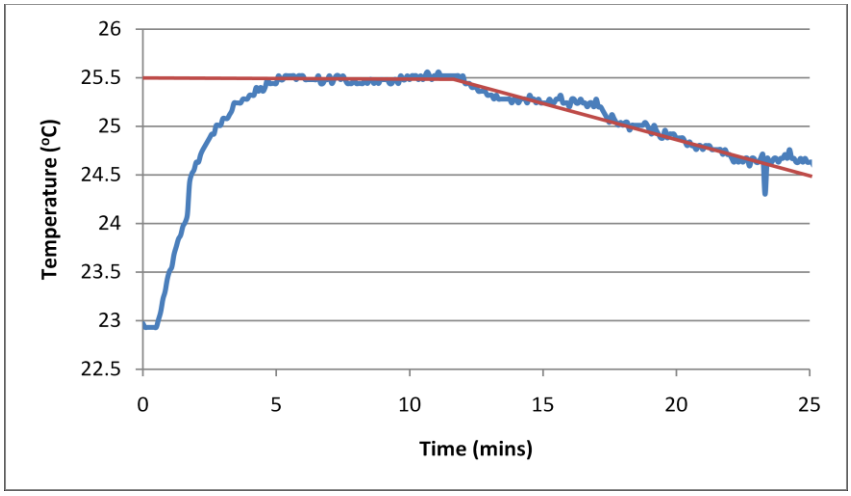

Figure 3-2. Calibration of oscillating magnetic field instrument with water. The blue line shows the temperature of the solution. The red line represents the background temperature of the circulating oil.

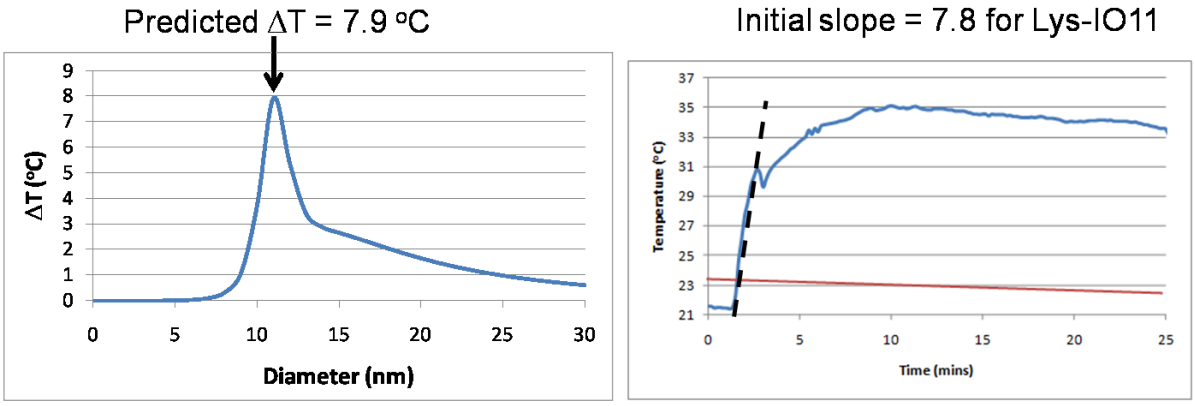

Figure 3-3. (a) Theoretical prediction of temperature rise vs. particle size assuming 1 nm-thick coating at 1 MHz frequency and 10.5 kA/m magnetic field after 1 minute, and (b) experimental temperature rise from 10 mg/mL 11 nm Fe_3O_4 nanoparticles

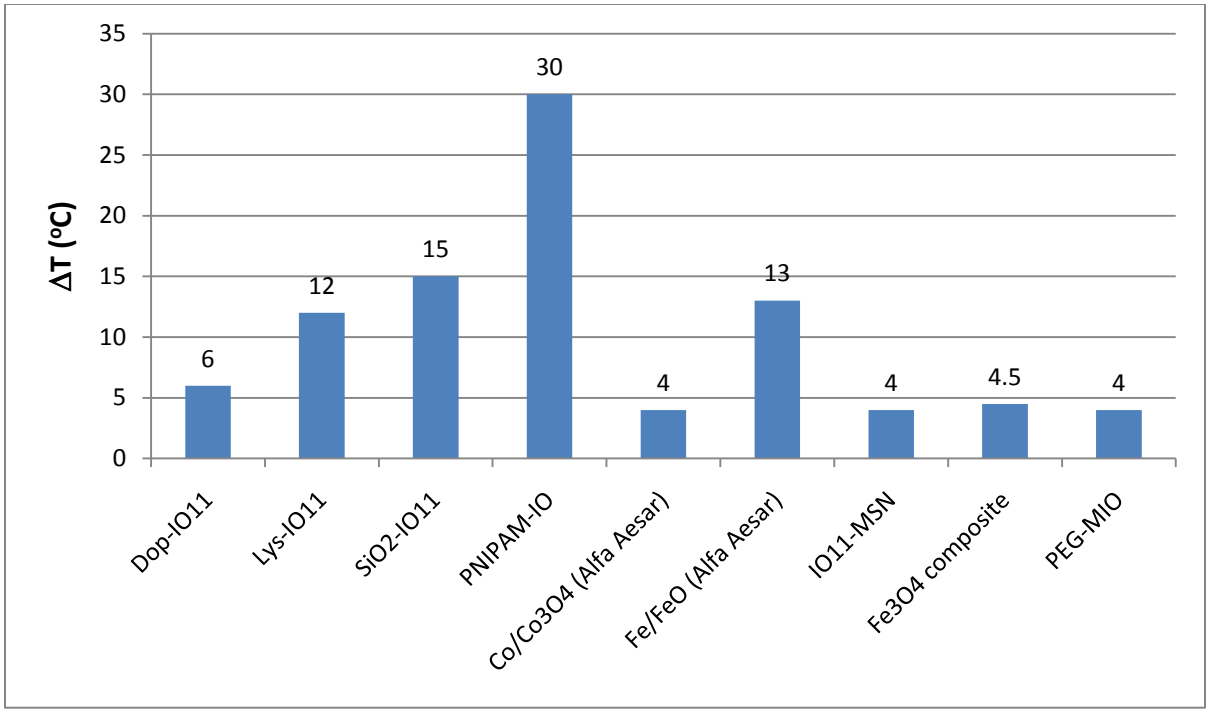

Figure 3-4. Normalized temperature rise (^{o}C) of aqueous suspensions with 10 mg/mL of various magnetic materials were compared under 10 kA/m magnetic field at 1 MHz frequency.

Sample list

Dop-IO11: Dopamine-coated 11 nm iron oxide nanoparticles

Lys-IO11: Lysine-coated 11 nm iron oxide nanoparticles

SiO_2-IO11: Silica-coated 11 nm iron oxide nanoparticles (4-6 nm thick)

PNIPAM-IO11: Poly-*N*-isopropylacrylamide coated iron oxide nanoparticles

Co/Co_3O_4: Commercial 5-15 nm cobalt nanoparticles with cobalt oxide shell

Fe/FeO: Commercial 10-30 nm iron nanoparticles with iron (II) oxide shell

IO11-MSN: 11 nm iron oxide nanoparticles embedded mesoporous silica nanoparticles

Fe_3O_4 composite: Composite of MCM-48 type silica with iron oxide in the pores

PEG-MIO: Poly(ethylene glycol) coated mesoporous iron oxides

Effect of coating: PNIPAM

Among the various coatings tested in this study, the most intriguing result is that of the PNIPAM-coated sample. According to the theoretical model, as outlined in Chapter 1 of this thesis, the heat generation from this sample should be rather ineffective compared to other samples for several reasons. First of all, the co-precipitation method produces Fe_3O_4 nanoparticles with broader size distribution than the high temperature method that yielded the 11-nm particles. Secondly, uncontrolled polymerization of NIPAM results in thick coating of polymer. Despite these "handicaps", the PNIPAM-coated sample shows the highest heating under the magnetic field among the samples evaluated in this study (Figure 3-4), which would suggest that relaxation mechanisms alone cannot account for the intense amount of heating observed. The rationale for this is still unclear at present time

Besides the Néel and Brown relaxation mechanisms, 2 other heat loss mechanisms are known: eddy current and hysteresis loss. Since magnetite is known to be non-conducting, induction of eddy current within the sample should be negligible. Aggregation of the sample, as the bulk temperature rises above the LCST of PNIPAM (32 ^{o}C), could result in some interactions between the Fe_3O_4 nanoparticles. The effect of magnetic interactions on the SLP is still a poorly understood issue in the theory of hyperthermia, especially when clusters are present.[18] Eggeman and co-workers found that clustered magnetite nanoparticles exhibited significant hysteresis.[19] In fact, the researchers found that under the oscillating magnetic field of 10 mT (about 8 kA/m) at 140 kHz, the clustered sample heated by up to 25 ^{o}C in 1000 s, while the well-dispersed sample at similar concentration showed no measurable heating. Following this argument, we speculate that hysteresis loss might also be present in

our PNIPAM-IO sample as well. However, further evaluation of cluster size in solution and magnetization is needed to confirm this effect.

Effect of mesoporous support & structures

Embedding 11 nm Fe_3O_4 nanoparticles inside mesoporous silica (IO11-MSN) reduces the temperature rise of the solution compared to free-floating iron oxide nanoparticles (Figure 3-4). Since the iron oxide nanoparticles are anchored within the mesoporous support, the movement of the particles should be constricted and thus we expect the Néel relaxation to be the principal heat loss mechanism for this system. The limitation of Brown relaxation may partially account for the relatively low SLP. At first glance, it may also seem that the 4 wt% of Fe loading may account for this effect. However, filling all the pore channels with Fe_3O_4, as in the Fe_3O_4 composite sample, does not result in a significant increase in SLP. Moreover, mesoporous Fe_3O_4 also yields similar result as IO11-MSN, which is an indication that increasing Fe content in mesostructures may not improve the SLP very much under the prescribed condition. It is interesting to note that there must be some clustering as well in the mesoporous iron oxides, however this arrangement did not yield higher SLP from this system.

Effect of the type of materials

As mentioned in Chapter 1 of this thesis, superparamagnetic nanoparticles (e.g. small Fe_3O_4 nanoparticles) generate heat only through relaxation mechanisms. To assess the effect of hysteresis loss mechanism, commercial ferromagnetic 10-30 nm Fe(core)/FeO(shell) and 5-15 nm Co(core)/Co_3O_4(shell) nanoparticles were evaluated under oscillating magnetic field. Under the condition tested, the iron nanoparticles generated more heat under

oscillating magnetic field than the Co but are only comparable to the lysine-coated iron oxide nanoparticles. In order to maximize the SLP of the iron nanoparticles, the magnetization properties of this material will be investigated and the oscillating magnetic field conditions adjusted accordingly.

Synthesis of 7-hydroxycoumarin-3-carboxylic acid under oscillating magnetic field

Scheme 1

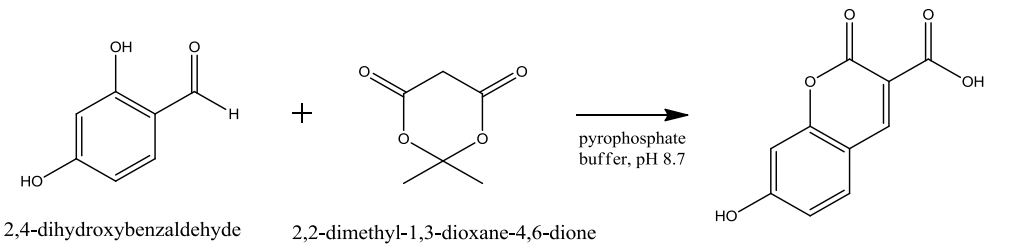

2,4-dihydroxybenzaldehyde 2,2-dimethyl-1,3-dioxane-4,6-dione 7-hydroxycoumarin-3-carboxylic acid

The synthesis of 7-hydroxycomarin-3-carboxylic acid from 2,4-dihydroxybenzaldehyde and Meldrum's acid (Scheme 1) in pyrophosphate buffer proceeded slowly at room temperature and was accelerated at higher temperatures (Figure S1) in the first 4 hours. The reaction rate, however, dropped faster at high temperature due to the faster degradation of the dihydroxybenzaldehyde. While the reaction yield was not very high, the difference in initial kinetics of the reaction was sufficient for our purposes. Thus, the subsequent reactions were evaluated only within the first 4 hours of the reaction time.

For oscillating magnetic field tests, magnetic nanoparticles were added to the reaction solutions and exposed to AC magnetic field at 10.5 kA/m and 1 MHz frequency. For this preliminary study, the iron oxide-embedded MSN (IO11-MSN) and PNIPAM-coated iron oxides (PNIPAM-IO) were chosen to represent the least and the most effective materials in raising the bulk solution temperature under oscillating magnetic field (Figure 3-4). 20

mg/mL IO11-MSN only raised the bulk solution temperature of the reaction by 4 ^{o}C (Figure 3-5c), thus the control reaction was performed at room temperature (Figure 3-5a). With the IO11-MSN, the reaction yield under oscillating magnetic field was the same as the control after the first hour and only increased by 1% after 3 hours (Figure 3-5a).

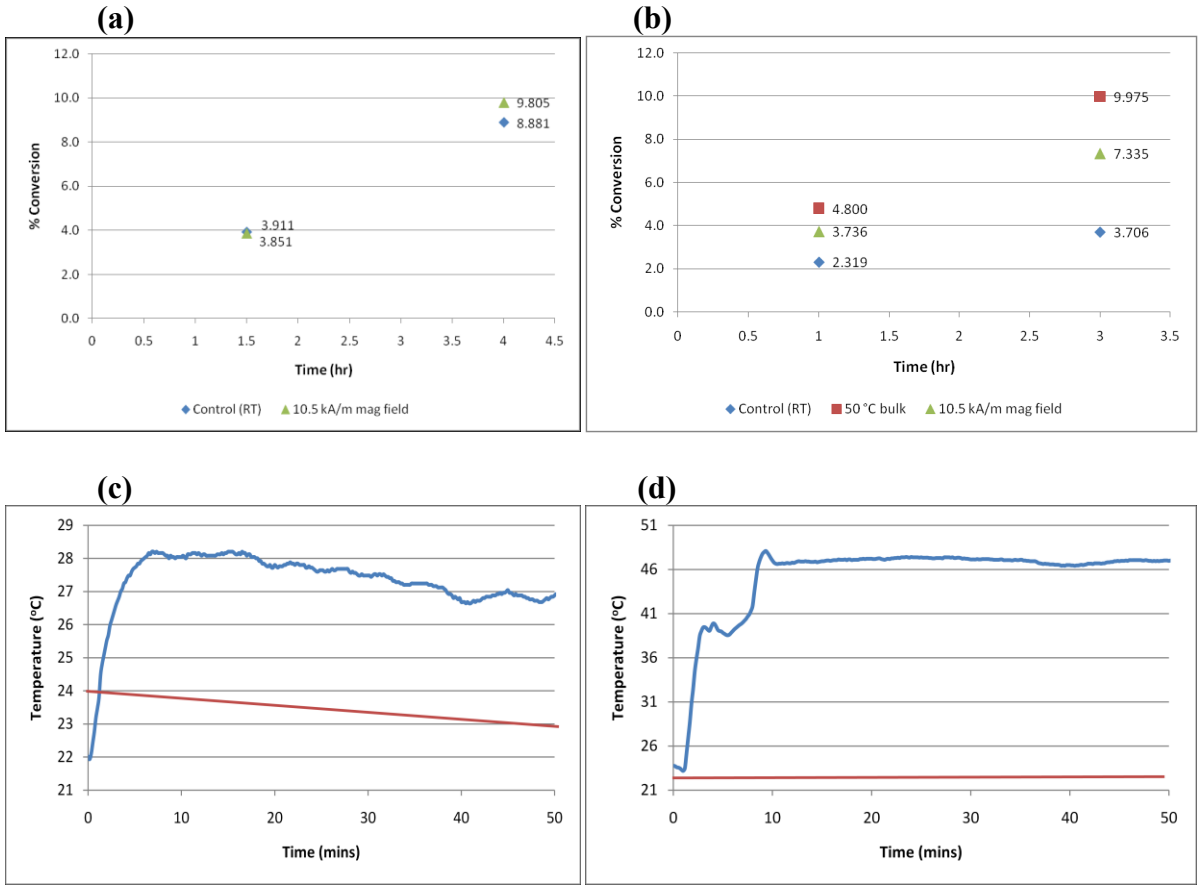

Figure 3-5. % conversion of the 2,4-dihydroxybenzaldehyde to 7-hydroxycoumarin-3-carboxylic acid (a) with 20 mg/mL IO11-MSN and (b) with 10 mg/mL PNIPAM-IO are compared at room temperature, under 10.5 kA/m oscillating magnetic field at 1 MHz frequency, and with bulk heating (oil bath). The temperatures of the bulk solutions under oscillating magnetic field are recorded *in situ* for (c) reaction with IO11-MSN and (d) with PNIPAM-IO; the blue lines represent solution temperature and red lines represent the background temperature of the circulating oil.

With 10 mg/mL PNIPAM-IO, the reaction yield in an oscillating magnetic field was higher than to the room temperature control after the first hour and doubled after 3 hours (Figure 3-5b). This result was encouraging in that the reaction could be accelerated under an oscillating magnetic field using this system. However, further testing revealed that the oscillating magnetic field system was not as effective as the bulk heating. The bulk solution of the reaction was raised to around 47 ^{o}C (Figure 3-5d) under an oscillating magnetic field, thus another control reaction was performed by heating the reaction mixture to 50 ^{o}C in an oil bath. Compared to the oscillating magnetic field system, the bulk heating resulted in higher yield even after the first hour (Figure 3-5b). In this case, the local heating did not have an enhanced effect over bulk heating because the oscillating magnetic field heating is not as uniform as bulk heating. The nanoparticles tended to cluster and precipitate over time, thus concentrating heat generation by oscillating magnetic field to the bottom of the tube.

Conclusions

Various magnetic materials were evaluated for their abilities to raise the solution temperature in 10.5 kA/m oscillating magnetic field at 1 MHz frequency. The heat loss by 11 nm magnetite nanoparticles matched the theoretical prediction very well when the surface ligand was lysine, but not when the surface coating was changed. Coating species had a tremendous effect on the temperature rise of the nanoparticles; most notably, PNIPAM-coated iron oxide was able to raise the solution temperature by 30 ^{o}C. This amount of heat loss is much higher than permissible by the predicted theories involving only the relaxation mechanisms for particles under our condition. Effects of magnetic interactions through particle clustering might contribute to the high temperature rises of PNIPAM-IO and SiO_2-

IO, but more testing is needed to confirm this effect. The mesoporous materials tested here were not as effective in raising the solution temperatures, compared to free-floating nanoparticles.

An oscillating magnetic field was also applied to the uncatalyzed synthesis of 7-hydroxycoumarin-3-carboxylic acid. Oscillating magnetic field heating was effective in accelerating the reaction when compared to room temperature control, but was less effective than bulk heating at comparable solution temperature. More systems to harness the heat generated from nanoparticles functionalized with catalytic systems are being studied.

References

(1) Hergt, R.; Dutz, S.; Müller, R.; Zeisberger, M. *Journal of Physics: Condensed Matter* 2006, *18*, S2919.

(2) Pankhurst, Q. A. *Journal of physics. D, Applied physics* 2003, *36*, 167.

(3) Higai, K.; Masuda, D.; Matsuzawa, Y.; Satoh, T.; Matsumoto, K. *Biological & Pharmaceutical Bulletin* 1999, *22*, 333-338.

(4) Perry, J. D.; James, A. L.; Morris, K. A.; Oliver, M.; Chilvers, K. F.; Reed, R. H.; Gould, F. K. *Journal of Applied Microbiology* 2006, *101*, 977-985.

(5) Horst, M. A. v. d.; Stalcup, T. P.; Kaledhonkar, S.; Kumauchi, M.; Hara, M.; Xie, A.; Hellingwerf, K. J.; Hoff, W. D. *Journal of the American Chemical Society* 2009, *131*, 17443-17451.

(6) Holeman, L. A.; Robinson, S. L.; Szostak, J. W.; Wilson, C. *Folding & Design* 1998, *3*, 423-431.

(7) Kiyokawa, T.; Kanaori, K.; Tajima, K.; Kawaguchi, M.; Mizuno, T.; Oku, J.-i.; Tanaka, T. *Chemistry--A European Journal* 2004, *10*, 3548-3554.

(8) Cave, G. W. V.; Raston, C. L.; Scott, J. L. *Chemical Communications (Cambridge, United Kingdom)* 2001, 2159-2169.

(9) Scott, J. L.; Raston, C. L. *Green Chem.* 2000, *2*, 245-247.

(10) Maggi, R.; Bigi, F.; Carloni, S.; Mazzacani, A.; Sartori, G. *Green chemistry* 2001, *3*, 173-174.

(11) Du, J.-L.; Li, L.-J.; Zhang, D.-H. *E-Journal of Chemistry* 2006, *3*, 1-4.

(12) Babincova, M.; Cicmanec, P.; Altanerova, V.; Altaner, C.; Babinec, P. *Bioelectrochemistry* 2002, *55*, 17-19.

(13) Tai, L.-A.; Tsai, P.-J.; Wang, Y.-C.; Wang, Y.-J.; Lo, L.-W.; Yang, C.-S. *Nanotechnology* 2009, *20*, 135101/1-135101/9.

(14) Ghosh, S.; Neogi, A.; Yang, C.; Cai, T.; GhoshMitra, S.; Diercks, D.; Hu, Z. *Materials Research Society Symposium Proceedings* 2008, *1095E*, Paper #: 1095-EE03-20.

(15) Hoare, T.; Santamaria, J.; Goya, G. F.; Irusta, S.; Lin, D.; Lau, S.; Padera, R.; Langer, R.; Kohane, D. S. *Nano Lett.* 2009, *9*, 3651-3657.

(16) Derfus, A. M.; von Maltzahn, G.; Harris, T. J.; Duza, T.; Vecchio, K. S.; Ruoslahti, E.; Bhatia, S. N. *Advanced Materials* 2007, *19*, 3932-3936.

(17) Hawkins, A. M.; Satarkar, N. S.; Hilt, J. Z. *Pharmaceutical Research* 2009, *26*, 667-673.

(18) Hergt, R.; Dutz, S.; Röder, M. *Journal of Physics: Condensed Matter* 2008, *20*, 385214.

(19) Eggeman, A. S.; Majetich, S. A.; Farrell, D.; Pankhurst, Q. A. *IEEE Transactions on Magnetics* 2007, *43*, 2451-2453.

Appendix

Supporting information

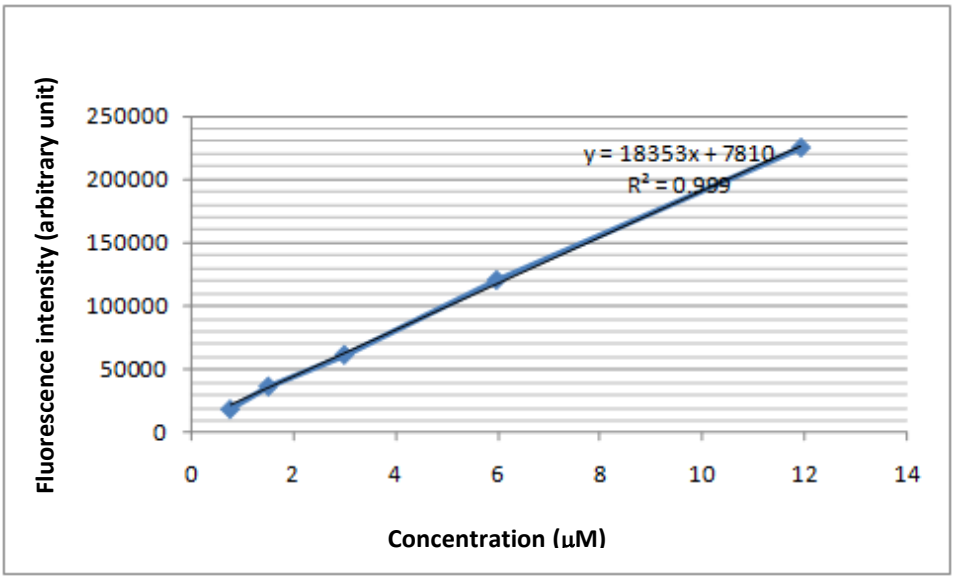

Figure S1: Standard calibration curve of 7-hydroxycoumarin-3-carboxylic acid in 0.083 M pyrophosphate buffer, pH 8.7.

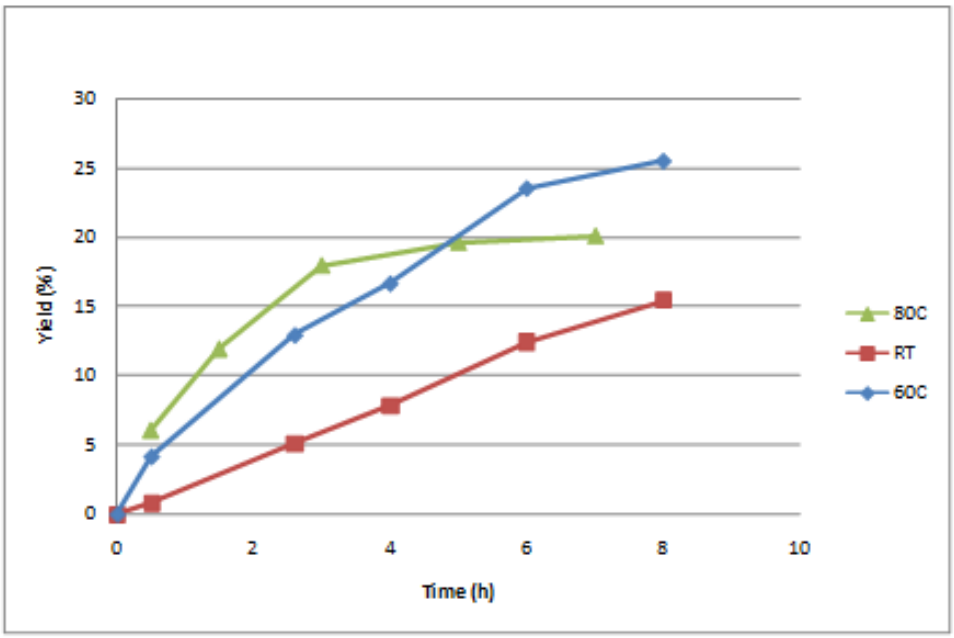

Figure S2: Effect of the temperature on the reaction yield of the synthesis of 7-hydroxycoumarin-3-carboxylic acid in 0.083 M pyrophosphate buffer, pH 8.7.